

# AC Voltage Generation by Spin Pumping and Inverse Spin Hall Effect

HuJun Jiao<sup>1</sup> and Gerrit E. W. Bauer<sup>2,1</sup>

<sup>1</sup>*Kavli Institute of NanoScience, Delft University of Technology, 2628 CJ Delft, The Netherlands*

<sup>2</sup>*Institute for Materials Research, Tohoku University, Sendai 980-8577, Japan*

(Dated: August 6, 2018)

The polarization of the spin current pumped by a precessing ferromagnet into an adjacent normal metal has a constant component parallel to the precession axis and a rotating one normal to the magnetization. The former component is now routinely detected in the form of a DC voltage induced by the inverse spin Hall effect (ISHE). Here we compute AC-ISHE voltages much larger than the DC signals for various material combinations and discuss optimal conditions to observe the effect. Including the backflow of spins is essential for distilling parameters such as the spin Hall angle from ISHE-detected spin pumping experiments.

PACS numbers:

In magnetoelectronics the electronic spin degree of freedom creates new functionalities that lead to applications in information technologies such as sensors and memories [1]. Central to much excitement in this field is the spin Hall effect (SHE) [2–5], *i.e.* the spin current induced normally to an applied charge current in the presence of spin-orbit interaction, as discovered optically in semiconductors [6, 7] and subsequently electrically in metals [8–10]. Recently magnetization reversal by the SHE induced spin transfer torque has been demonstrated [11]. The generation of a voltage by a spin current injected into a paramagnetic metal, the *inverse* spin Hall effect (ISHE), can be employed to detect the spin current due to spin-pumping [12–14] by an adjacent ferromagnet under ferromagnetic resonance (FMR) conditions [8, 15]. The ISHE has also been essential for the discovery of the spin Seebeck effect [16].

In recent experiments, DC voltages induced by the ISHE have been measured in many material combinations thereby giving access to crucial parameters such as the spin Hall angle [17–19] and the spin mixing conductance [20], *i.e.* the material parameter determining the effectiveness of interface spin-transfer torques [13]. For example, the magnitude and sign of the ISHE as parameterized by the spin Hall angle has been determined for permalloy (Py)|N bilayers for different normal metals N [17, 18]. An approximate scaling relation for the spin pumping by numerous ferromagnets (F) has been discovered by comparing different F|Pt bilayers as a function of excitation power [20]. However, it is far from easy to derive quantitative information from ISHE experiments [21]. As reviewed by the Cornell collaboration [22], several experimental pitfalls should be avoided. At the FMR, the DC ISHE voltage is small, scaling quadratically with the cone angle of the precessing magnetization. An important correction is caused by the back-diffusion (“back-flow”) of injected spins to the interface, which effectively reduces the spin current injection [13] and generates voltages normal to the interface [23, 24]. This backflow has often been neglected in interpreting

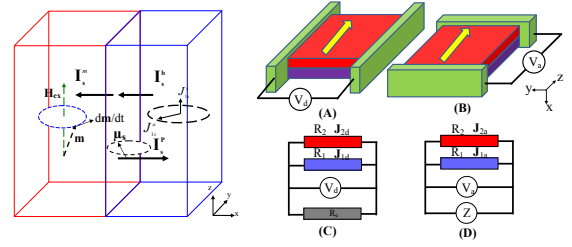


FIG. 1: Schematic spin battery operated by FMR, including the measurement configurations (A and B), and their equivalent circuits (C and D). The AC(DC) voltage between both ends of the sample drops along the  $z(y)$  direction.  $R_{1,2}$  in the equivalent circuit represents the resistances of the normal metal and the ferromagnet, respectively.  $J_{1(2)d(a)}$  denote the DC (AC) charge current due to the ISHE in the normal metal (1) or ferromagnet (2).  $R_e$  is a parasitic resistance in the external circuit for the DC, while  $Z$  is the external impedance for the AC measurements.

spin pumping experiments, assuming that Pt, the metal of choice, can be treated like a perfect spin sink.

The spin current injected by FMR into a normal metal consists of a DC component along the  $z$ -axis parallel to the effective field and an AC component normal to it, *i.e.* in the  $xy$ -plane (see Fig. 1). In this Letter we analyze both AC and DC ISHE voltages by time-dependent spin diffusion theory, where the former is generated between the edges of the sample along the  $z$ -direction, *i.e.* for a different sample configuration than used for DC signal detection. For small precession angles the AC ISHE voltage is found to be orders of magnitude larger than the DC signal. The back-flow of spins modifies also the DC voltage even for small spin-flip diffusion lengths, requiring a reappraisal of published parameters.

A normal metal N in contact with a ferromagnet F under FMR as shown in Fig. 1 can be interpreted as a spin battery [25]. When the ferromagnetic film is thicker than its transverse spin-coherence length (a few monolayers),

the adiabatically pumped spin current reads [12–14, 25]

$$\mathbf{I}_s^p = \frac{\hbar}{4\pi} \left( \text{Re} g^{\uparrow\downarrow} \mathbf{m} \times \frac{d\mathbf{m}}{dt} + \text{Im} g^{\uparrow\downarrow} \frac{d\mathbf{m}}{dt} \right), \quad (1)$$

where  $\mathbf{m}$  is the unit vector of the magnetization direction and  $g^{\uparrow\downarrow}$  is the (dimensionless) complex spin mixing conductance [26]. The pumping spin current creates a spin accumulation in N that induces a diffusion backflow of spins into F:

$$\mathbf{I}_s^b = \frac{g}{8\pi} [2p(\mu_0^F - \mu_0^N) + \mu_s^F - \mathbf{m} \cdot \boldsymbol{\mu}_s^N] \mathbf{m} - \frac{\text{Re} g^{\uparrow\downarrow}}{4\pi} \mathbf{m} \times (\boldsymbol{\mu}_s^N \times \mathbf{m}) + \frac{\text{Im} g^{\uparrow\downarrow}}{4\pi} \mathbf{m} \times \boldsymbol{\mu}_s^N, \quad (2)$$

where  $\mu_0^N, \boldsymbol{\mu}_s^N$  in N and  $\mu_0^F, \mu_s^F \mathbf{m}$  in F are the charge and spin accumulations at the interface. The sum of spin-up and spin-down interface conductances is the total conductance  $g = g^{\uparrow\uparrow} + g^{\downarrow\downarrow}$  with  $p = (g^{\uparrow\uparrow} - g^{\downarrow\downarrow}) / (g^{\uparrow\uparrow} + g^{\downarrow\downarrow})$  the conductance spin polarization. The magnetization determined by the Landau-Lifshitz-Gilbert equation is assumed to precess with constant cone angle  $\theta$  around the  $z$ -axis, whose magnitude is governed by the rf radiation intensity. The spin accumulation in N obeys the spin-diffusion equation [27]

$$\frac{\partial \boldsymbol{\mu}_s^N(\mathbf{r}, t)}{\partial t} = \gamma_N \mathbf{H}_{ex} \times \boldsymbol{\mu}_s^N + D_N \frac{\partial^2 \boldsymbol{\mu}_s^N}{\partial x^2} - \frac{\boldsymbol{\mu}_s^N}{\tau_{sf}^N}, \quad (3)$$

where  $\gamma_N$  is the gyromagnetic ratio,  $D_N$  the diffusion constant and  $\tau_{sf}^N$  the spin-flip relaxation time, all in N. The spin current  $\mathbf{I}_s = \mathbf{I}_s^p + \mathbf{I}_s^b$  is continuous at the N|F interface and vanishes at the outer boundary  $x = d_N$ . In position-frequency space the exact solution for the spatiotemporal dependence of the spin accumulation reads

$$\boldsymbol{\mu}_s^N(x, \omega) = \sum_{i=1}^3 \vec{v}_i \frac{\cosh[\kappa_i(x - d_N)]}{\sinh[\kappa_i d_N]} \frac{2j_s^i(x=0, \omega)}{\hbar \nu D_N \kappa_i}. \quad (4)$$

$\kappa_1^2(\omega) = (1 + i\omega\tau_{sf}^N)/(\lambda_{sd}^N)^2$ ,  $\kappa_{2,3}^2(\omega) = \kappa_1^2(\omega) \pm iC$ ,  $C = -\gamma_N H_{ex}/D_N$  and  $\lambda_{sd}^N = \sqrt{D_N \tau_{sf}^N}$ .  $j_{1s} = I_s^z/A$  and  $j_{(2,3)s} = (I_{xs} \pm iI_{ys})/(\sqrt{2}A)$  are spin current densities, where  $A$  is the interface area. Three eigenvectors associated with  $\kappa_i^2(\omega)$  ( $i = 1, 2, 3$ ) are, respectively,  $\vec{v}_1 = (0 \ 0 \ 1)$ ,  $\vec{v}_2 = (1 \ -i \ 0)/\sqrt{2}$ ,  $\vec{v}_3 = (1 \ i \ 0)/\sqrt{2}$ . In position-time domain

$$\mathbf{j}_{1s}(x, t) = -\frac{\hbar \nu D_N}{2} \frac{\partial \boldsymbol{\mu}_s^N(x, t)}{\partial x} = j_{1s}^z(x) \mathbf{e}_z + \mathbf{j}_{1s}^a(x, t), \quad (5)$$

with

$$j_{1s}^z(x) \mathbf{e}_z = \frac{\sinh[\kappa_1(0)(d_N - x)]}{\sinh[\kappa_1(0)d_N]} j_{1s}^z(0) \mathbf{e}_z, \quad (6)$$

$$\mathbf{j}_{1s}^a(x) = 2 \text{Re} \left\{ \frac{\sinh[\kappa_2(\omega)(d_N - x)]}{\sinh[\kappa_2(\omega)d_N]} \mathbf{j}_{1s}^a(0) e^{i\omega t} \right\} \quad (7)$$

$j_{1s}^z(0)$  and  $\mathbf{j}_{1s}^a(0)$  are complicated analytic expression (not shown) for the DC and AC components of the spin current at the N-side of the interface.

The longitudinal component of the spin accumulation can penetrate into a metallic ferromagnet, leading to a spin accumulation  $\mathbf{m}(t)\mu_s^F$ .  $\mu_s^F = \mu_{\uparrow}^F - \mu_{\downarrow}^F$  that satisfies the spin-diffusion equation

$$\frac{\partial^2 \mu_s^F(x)}{\partial x^2} = \frac{\mu_s^F(x)}{(\lambda_{sd}^F)^2}, \quad (8)$$

where  $\lambda_{sd}^F$  is the spin-flip diffusion length in the ferromagnet. In an open circuit the DC charge current vanishes and we obtain

$$\mu_s^F(x) = \frac{\cosh[(d_F + x)/\lambda_{sd}^F] \tilde{g}}{[g_F \tanh[d_F/\lambda_{sd}^F] + \tilde{g}] \cosh[d_F/\lambda_{sd}^F]} \mathbf{m} \cdot \boldsymbol{\mu}_s^N, \quad (9)$$

where  $g_F = 4hA\sigma_{\uparrow}\sigma_{\downarrow}/[e^2\lambda_{sd}^F(\sigma_{\uparrow} + \sigma_{\downarrow})]$ ,  $\tilde{g} = (1 - p^2)g$ . Here,  $\sigma_{\uparrow(\downarrow)}$  is the conductivity of spin-up(-down) electrons in F. The spin current density in F reads

$$\mathbf{j}_{2s}(x) = \frac{\sinh[(d_F + x)/\lambda_{sd}^F]}{\sinh[d_F/\lambda_{sd}^F]} \mathbf{j}_{2s}(0). \quad (10)$$

At the interface

$$\mathbf{j}_{2s}(0) = -\frac{1}{8\pi} \frac{\tilde{g} g_F \tanh[d_F/\lambda_{sd}^F]}{\tilde{g} + g_F \tanh[d_F/\lambda_{sd}^F]} (\mathbf{m} \cdot \boldsymbol{\mu}_s^N) \mathbf{m}. \quad (11)$$

When spin-flip in F is negligible,  $\lambda_{sd}^F \gg d_F$ ,  $\mu_s^F(0) = \mathbf{m} \cdot \boldsymbol{\mu}_s^N$  and the spin current in F vanishes. The backflow spin current modifies the magnetization dynamics by contributing a three-component transfer torque that (i) reduces the interface Gilbert damping due to spin pumping, (ii) modulates the gyromagnetic ratio, and (iii) adds an effective magnetic field. For the system parameters considered below the last two terms are too small to affect the magnetizations dynamics, however.

The ISHE generates a charge current transverse to an applied spin current due to the spin-orbit interaction, which for in an open circuit generates electric fields. With spin current along the  $x$ -direction, the charge current reads [8, 15, 17–20]

$$\mathbf{j}_c(x) = \alpha_{N/F} (2e/\hbar) \mathbf{e}_x \times \mathbf{j}_s(x), \quad (12)$$

where  $\alpha_N$  is the spin Hall angle in N and  $\alpha_F = (\alpha_{F\uparrow} + \alpha_{F\downarrow})/2$  is that in F, where  $\alpha_{F\xi} = \sigma_{AH\xi}/\sigma_{\xi}$  ( $\xi = \uparrow, \downarrow$ ) and  $\sigma_{(AH)\xi}$  is the spin-polarized (anomalous Hall) conductivity.

As shown in Fig. 1(A) (1(B)), a DC (AC) component can be detected along the  $y$  ( $z$ ) direction by the electric fields  $E_y \mathbf{e}_y$  ( $E_z(t) \mathbf{e}_z$ ). We consider the equivalent circuits shown in Fig. 1(C) (1(D)) and disregard parasitic impedances, *i.e.* assume that  $R_e, Z \rightarrow \infty$ . In the steady

state, we obtain an AC electric field:

$$E_z(t) = \frac{4e/\hbar}{\sigma_N d_N + \sigma_F d_F} \text{Re} \left( \frac{\alpha_N j_{1s}^y(0)}{\kappa_2(\omega)} \tanh \frac{d_N \kappa_2(\omega)}{2} + \alpha_F j_{2s}^y(0) \lambda_{sd}^F \tanh \frac{d_N}{2\lambda_{sd}^N} \right). \quad (13)$$

The DC electric field along the  $y$ -direction reads

$$E_y = \frac{2e/\hbar}{\sigma_N d_N + \sigma_F d_F} \left[ j_{1s}^z(0) \alpha_N \lambda_{sd}^N \tanh \frac{d_N}{2\lambda_{sd}^N} + j_{2s}^z(0) \alpha_F \lambda_{sd}^F \tanh \frac{d_F}{2\lambda_{sd}^F} \right]. \quad (14)$$

These equations are our main results. In the following we disregard  $\text{Im} g^{\uparrow\downarrow}$  which is small for the interfaces considered below. When backflow is disregarded we recover the relation [17, 18]

$$E_y^{NB} = \frac{e\alpha_N f_{FMR} \sin^2 \theta \text{Re} g^{\uparrow\downarrow}}{\sigma_N d_N + \sigma_F d_F} \frac{\lambda_{sd}^N}{A} \tanh \frac{d_N}{2\lambda_{sd}^N}. \quad (15)$$

as well as the AC signal

$$\frac{E_z^{NB}(t)}{\cos(\omega t + \delta)} = \frac{e\alpha_N f_{FMR} \sin \theta \text{Re} g^{\uparrow\downarrow}}{\sigma_N d_N + \sigma_F d_F} \frac{1}{A} \left| \frac{\tanh[\kappa_2(\omega) d_N/2]}{\kappa_2(\omega)} \right|, \quad (16)$$

where  $\delta = \delta_0 + \text{Arg}\{\tanh[\kappa_2(\omega) d_N/2]/\kappa_2(\omega)\}$ , with  $\delta_0 = -\pi$  for  $\alpha_N > 0$  and  $0$  for  $\alpha_N < 0$ , is the phase shift relative to the ac excitation field  $\cos(\omega t) \mathbf{e}_y$ .

The spin-pumping induced spin accumulation is governed by two length scales,  $\lambda_{sd}^N$  and the transverse spin dephasing length  $\lambda_c = \sqrt{D_N/\omega}$  [13]. For  $x \ll \lambda_c$  the spin accumulation follows rigidly the instantaneous  $\mathbf{m} \times \dot{\mathbf{m}}$  polarization and contributions to both AC and DC ISHE are large. When  $x \gg \lambda_c$  the transverse component is dephased such that only a time-independent  $\mathbf{e}_z$  component remains [25] that contributes to the DC, but not the AC signal. From  $\omega \ll 1/\tau_{sf}^N$  follows  $\lambda_{sd}^N \ll \lambda_c$ . This is the case when  $\omega \tau_{sf}^N \simeq 0.2 (f_{FMR}/10 \text{ GHz}) (\tau_{sf}^N/3 \text{ ps}) \ll 1$ .  $\omega \tau_{sf}^N = 1 \times 10^{-3}$  in Pt and  $1.5 \times 10^{-2}$  in Ta at  $f_{FMR} = 15.5 \text{ GHz}$  with  $\tau_{sf}^{Pt} = 0.01 \text{ ps}$  and  $\tau_{sf}^{Ta} = 0.15 \text{ ps}$  calculated from the data in Table I. So in the present frequency region this condition is fulfilled for strongly spin-dissipating metals. The diffusive dephasing of the time-dependent spin accumulation is then small and the AC ISHE is maximal. In that limit the contribution from the anomalous Hall effect in a ferromagnet such as Py is found to be negligible. Previous expressions for the DC spin accumulation [13] and voltages [28, 29] agree with the present results in that limit. Note that this condition does not hold for metals with long spin-flip times for example single crystal Al.

In Fig. 2, we plot the DC electric fields with backflow of spin as a function of spin Hall angle  $\alpha_N$  and spin diffusion length  $\lambda_{sd}^N$  (noting that the results are very insensitive to changes in  $\lambda_{sd}^F$  and  $\alpha_F$ ). The strong correlation

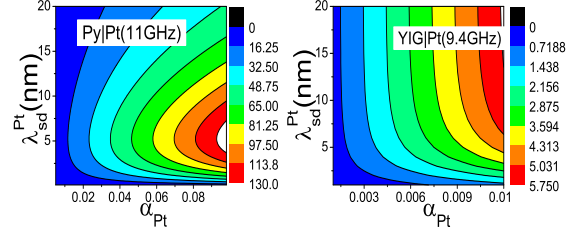


FIG. 2: The calculated DC field (in units of  $\mu\text{V}/\text{mm}$ ) as a function of the spin Hall angle and the spin-diffusion length (with backflow).

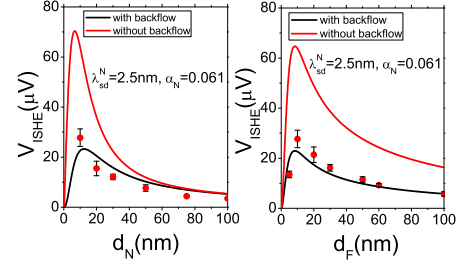


FIG. 3: Theoretical and experimental [28] ISHE voltages in Pt|Py bilayers as a function of Pt thickness (A) and Py thickness (B).

between these two parameters especially for YIG|Pt is evident. Nevertheless, we can narrow them down when also the Gilbert damping enhancement is measured, as was done recently by Nakayama *et al.* [28]. The spin-mixing conductance  $(\text{Re} g_{\text{eff}}^{\uparrow\downarrow}/A)^{-1} = (\text{Re} g^{\uparrow\downarrow}/A)^{-1} + \Gamma^{-1} = 3 \times 10^{19} \text{ m}^{-2}$  where  $\Gamma = (h/e^2)\sigma_N/\lambda_{sd}^N$  for  $d_N \gg \lambda_{sd}^N$  can be obtained from the Gilbert damping constant  $\zeta_{\text{eff}} = \zeta_0 + (g\mu_B)/(4\pi M_s d_F) \text{Re} g_{\text{eff}}^{\uparrow\downarrow}/A$ . The conductances are parameterized as  $\sigma_N = 4.1 \times (1 - e^{-d_N/29.6}) 10^6 \Omega^{-1} \text{ m}^{-1}$  and  $\sigma_F = 3.5 \times (1 - e^{-d_F/9.8}) 10^6 \Omega^{-1} \text{ m}^{-1}$  to fit the experiments (H. Nakayama, private communication). Since  $\text{Re} g^{\uparrow\downarrow} > 0$  the experiments provide the important constraint that  $\lambda_{sd}^N < 3.5 \text{ nm}$ , which is not consistent with larger values in use for this parameter. The constraint that the spin-flip scattering relaxation time should be larger than the scattering lifetime leads to  $\lambda_{sd}^N > 2 \text{ nm}$ . In Fig. 3 we plot the computed and the measured spin Hall voltages as a function of the layer thicknesses for optimized parameter combinations with and without backflow. The largest ISHE voltages are generated for  $d_N \simeq \lambda_{sd}^N$  (see below) [19, 28, 29]. Since above estimates favor  $\lambda_{sd}^N \approx 2.5 \text{ nm}$ , we estimate the Hall angle  $\alpha_{Pt} \approx 0.061$  from the spin pumping experiments [28] and consistency arguments alone. These parameters are different from those reported [19, 28], illustrating the importance of taking into account the experimental constraint on  $\lambda_{sd}^N$  provided by the increased Gilbert damping.

In Fig. 4 we turn to the AC-ISHE by comparing its

TABLE I: Parameters for selected bilayer systems used to compute AC ISHE electric fields induced by spin pumping under FMR.

N	$^a \nu_{DOS}$ [ $10^{47} J^{-1} m^{-3}$ ]	$\sigma_N$ [ $10^6 \Omega^{-1} m^{-1}$ ]	$\lambda_{sd}^N$ [nm]	$\alpha_N$	$g_N^{sh}$ [ $10^{19} m^{-2}$ ]
Al	1.5	$^{b11}$	$^{b350}$	$^c 0.0001$	3.6
Ta	4.3	$^d 0.53$	$^e 2.7$	$^d -0.15$	2.5
Au	1.1	$^f 25.2$	$^f 35$	$^f 0.0035$	1.2
Pd	10.0	$^f 4.0$	$^f 15$	$^f 0.0064$	1.6
Pt	9.1	$^g 5$	$^g 1.5$	$^g 0.07$	1.8
<hr/>					
	Py NM	YIG Au	YIG Pt	p	
$\frac{Re g^{\uparrow\downarrow}}{A}$	$2g_N^{sh}$	$^h 0.66$	2.3	0.4	

$^a$ Ref. 32,  $^b$ Ref. 33,  $^c$ Ref. 9,  $^d$ Ref. 34,  $^e$ Ref. 35,  $^f$ Ref.17,  $^g$ Ref.22  
 $^h$ Ref. 36. Schep corrections[37, 38] are included in  $Re g^{\uparrow\downarrow}/A$ .

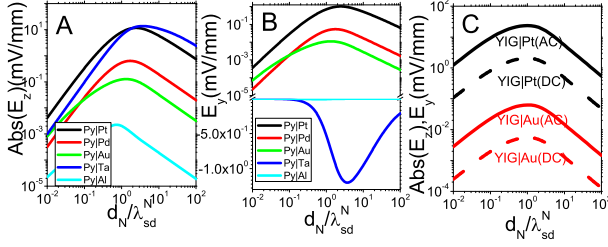


FIG. 4: The AC and DC electric fields as a function of  $d_N$  for Py|N and YIG|N for a fixed FMR frequency of 15.5 GHz. Here, the precession angle is  $5^\circ$  and  $d_F = 15$  nm.

dependence on the normal metal thickness with the DC counterpart for a precession angle of  $5^\circ$  for Py|N (N=Au, Ta, Pd, Pt and Al) and YIG|N (N=Pt,Au) bilayers. In Py, we choose the electrical conductivity  $\sigma_{Py} = 1.5 \times 10^6 \Omega^{-1} m^{-1}$  and the conductivity polarization  $q = (\sigma_{Py}^{\uparrow} - \sigma_{Py}^{\downarrow})/\sigma_{Py} = 0.7$ , estimate the spin Hall angle  $\alpha_{Py} = 0.076$  from the Hall electrical conductivity  $\sigma_H = 0.09 \times 10^6 \Omega^{-1} m^{-1}$ [30] and its polarization  $p_H = (\sigma_{H\uparrow} - \sigma_{H\downarrow})/\sigma_H = 0.5$ . Its spin-diffusion length is chosen as  $\lambda_{sd}^F = 5$  nm [31]. Both ISHE fields are maximized for  $d_N \sim \lambda_{sd}^N$  since the AC and DC signals are affected by two factors, *i.e.* the effective spin current and the effective resistance. Increasing  $d_N$  from zero, the total spin current initially increases exponentially because of the reduced backflow. When the thickness increases further, the emf generated by the ISHE close to the interface is short-circuited by the normal metal region  $x \gtrsim \lambda_{sd}^N$ , leading to an algebraic decrease of the voltage for larger  $d_N$ . A systematic experimental study of the DC ISHE as a function of  $d_N$  around the spin-diffusion length should help to understand the backflow and lead to a more accurate parameter determinations, including  $\lambda_{sd}^N$ .

We find that the anomalous Hall effect in Py caused by the backflow of spins into the ferromagnet is negligible unless the ISHE in the normal metal is very small, as *e.g.* in single crystal Al. In Py|N or YIG|N the phase shifts

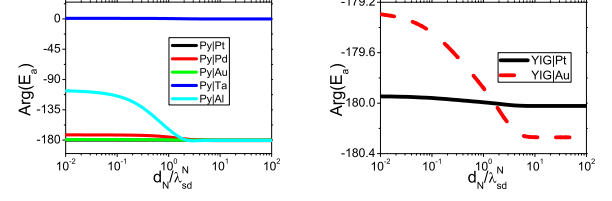


FIG. 5: Phase shift of the AC-ISHE relative to the rf magnetic field as function of  $d_N$  (with backflow).

depend only very weakly on  $d_N$ , again with the exception for a light metal such as Al. In Fig.5 we plot the phase of the AC-ISHE for selected bilayers. The phase difference of  $180^\circ$  at large  $d_N$  is simply caused by the different sign of the spin Hall angles for Pt(Pd,Au) and Ta. Again, interesting effects can be observed for a material with little spin dissipation such as Al, in which the phase is affected by the anomalous Hall effect in Py. For constant precession angles, the voltages increases with FMR frequency due to the increased spin pumping  $\sim |\mathbf{m}|$ . When the rf intensity is kept constant with frequency, the precession angle is inversely proportional to the FMR frequency. By increasing  $\omega$  for small cone angles the DC voltage therefore decreases, while the AC voltage is almost unchanged.

The AC voltage is proportional to the precession angle, or the square root of the AC excitation power, in contrast to the linear relation between DC voltage and excitation power [17, 18, 39]. Furthermore, the ratio of the AC to DC field moduli is much larger than unity for the intensities typical for FMR experiments. This ratio is close to a universal function as long as the anomalous Hall effect does not play a role (always the case for magnetic insulators) approaching the scaling function  $C(\omega) \cot \theta$ , where  $C(\omega)$  is material-dependent. When  $\omega \ll 1/\tau_{sf}^N$ ,  $C(\omega) \simeq 1$ , which is the case for Pt, Pd, Au and Ta.

In summary, we present a dynamical theory of the ISHE detection of spin pumping, explicitly including the back-diffusion of spins into the ferromagnet. We predict the generation of an AC voltage along the effective magnetic field in F|N bilayers under FMR. We predict magnitudes and phase shifts of the AC voltages for Py|N and YIG|N. From the analysis of published experiments, we predict that the spin Hall angle in Pt is 0.06. If the ISHE signal can be separated from parasitic voltages at the resonance frequency, the larger signals of AC measurements could be an attractive alternative to detect spin currents.

This work was supported by the FOM Foundation, EU-ICT-7 “MACALO”, the ICC-IMR, and DFG Priority Programme 1538 “Spin-Caloric Transport”. We thank Profs. Can-Ming Hu, Bechara Muniz, Sergio Rezende, and MinZhong Wu for their comments on the first version of the manuscript.



- 
- [1] S.D. Bader and S.S.P. Parkin, *Ann. Rev. Cond. Matt. Phys.* **1**, 71 (2010).
- [2] J. E. Hirsch, *Phys. Rev. Lett.* **83**, 1834 (1999).
- [3] S. Zhang, *Phys. Rev. Lett.* **85**, 393 (2000).
- [4] S. Murakami, N. Nagaosa, and S. C. Zhang, *Science* **301**, 1348 (2003).
- [5] J. Sinova, D. Culcer, Q. Niu, N. A. Sinitsyn, T. Jungwirth, and A. H. MacDonald, *Phys. Rev. Lett.* **92**, 126603 (2004).
- [6] Y. K. Kato, R. C. Myers, A. C. Gossard, D. D. Awschalom, *Science*, **306**, 1910(2004).
- [7] J. Wunderlich, B. Kaestner, J. Sinova, T. Jungwirth, *Phys. Rev. Lett.* **94**, 047204 (2005).
- [8] E. Saitoh, M. Ueda, H. Miyajima and G. Tatara, *Appl. Phys. Lett.* **88**, 182509 (2006).
- [9] S. O. Valenzuela and M. Tinkham, *Nature* **442**, 176 (2006).
- [10] T. Kimura, Y. Otani, T. Sato, S. Takahashi, and S. Maekawa, *Phys. Rev. Lett.* **98**, 156601 (2007).
- [11] L. Liu, C.-F. Pai, Y. Li, H.-W. Tseng, D. C. Ralph, R. A. Buhrman, *Science* **336**, 555 (2012)
- [12] Y. Tserkovnyak, A. Brataas, and G. E. W. Bauer, *Phys. Rev. Lett.* **88**, 117601 (2002).
- [13] Y. Tserkovnyak, A. Brataas, and G. E. W. Bauer, and B. Halperin, *Rev. Mod. Phys.* **77**, 1375 (2005).
- [14] F. S. M. Guimarães, A. T. Costa, R. B. Muniz, and D. L. Mills, *Phys. Rev. B* **84**, 054403 (2011)
- [15] A. Azevedo, L. H. Vilela Leão, R. L. Rodríguez-Suarez, A. B. Oliveira, and S. M. Rezende, *J. Appl. Phys.* **97**, 10C715 (2005).
- [16] K. Uchida, S. Takahashi, K. Harii, J. Ieda, W. Koshibae, K. Ando, S. Maekawa and E. Saitoh, *Nature* **455**, 778 (2008).
- [17] O. Mosendz, V. Vlaminc, J. E. Pearson, F.Y. Fradin, G. E.W. Bauer, S. D. Bader, and A. Hoffmann, *Phys. Rev. B* **82**, 214403 (2010).
- [18] O. Mosendz, J. E. Pearson, F.Y. Fradin, G. E.W. Bauer, S. D. Bader, and A. Hoffmann, *Phys. Rev. Lett.* **104**, 046601 (2010).
- [19] A. Azevedo, L. H. Vilela-Leão, R. L. Rodríguez-Suárez, A. F. Lacerda Santos, and S. M. Rezende, *Phys. Rev. B* **83**, 144402 (2011).
- [20] F. D. Czeschka, L. Dreher, M. S. Brandt, M. Weiler, M. Althammer, I.-M. Imort, G. Reiss, A. Thomas, W. Schoch, W. Limmer, H. Huebl, R. Gross, and S. T.B. Goennenwein, *Phys. Rev. Lett.* **107**, 046601 (2011).
- [21] Z. Feng, J. Hu, L. Sun, B. You, D. Wu, J. Du, W. Zhang, A. Hu, Y. Yang, D. M. Tang, B. S. Zhang, H. F. Ding, *Phys. Rev. B* **85**, 214423 (2012).
- [22] L. Liu, R. A. Buhrman, and D. C. Ralph, arXiv:1111.3702.
- [23] X. Wang, G. E.W. Bauer, Bart J. van Wees, Arne Brataas, and Yaroslav Tserkovnyak, *Phys. Rev. Lett.* **97**, 216602 (2006).
- [24] M. V. Costache, M. Sladkov, C.H. van der Wal, and B. J. van Wees, *Phys. Rev. Lett.* **97**, 216603 (2006).
- [25] A. Brataas, Y. Tserkovnyak, G. E.W. Bauer, and B. I. Halperin, *Phys. Rev. B* **66**, 060404(R) (2002).
- [26] A. Brataas, Yu. V. Nazarov, and G. E. W. Bauer, *Phys. Rev. Lett.* **84**, 2481 (2000); *Eur. Phys. J. B* **22**, 99 (2001).
- [27] M. Johnson and R. H. Silsbee, *Phys. Rev. B* **37**, 5312 (1988).
- [28] H. Nakayama, K. Ando, K. Harii, T. Yoshino, R. Takahashi, Y. Kajiwara, K. Uchida, Y. Fujikawa and E. Saitoh, *Phys. Rev. B* **85**, 144408 (2012).
- [29] V. Castel, N. Vlietstra, J. B. Youssef, and B. J. van Wees, arXiv:1206.7080 .
- [30] T. Miyasato, N. Abe, T. Fujii, A. Asamitsu, S. Onoda, Y. Onose, N. Nagaosa, and Y. Tokura, *Phys. Rev. Lett.*, **99**, 086602 (2007).
- [31] J. Bass and W.P. Pratt Jr., *J. Magn. Magn. Mater.* **200**, 274 (1999).
- [32] D.A. Papaconstantopoulos, *Handbook of the Band Structure of Elemental Solids* (Plenum, New York, 1986).
- [33] F. J. Jedema, H. B. Heersche, A. T. Filip, J. J. A. Baselmans, and B. J. van Wees, *Nature (London)* **416**, 713 (2002); M. Zaffalon and B. J. van Wees, *Phys. Rev. Lett.* **91**, 186601 (2003).
- [34] L. Liu, C.-F. Pai, Y. Li, H. W. Tseng, D. C. Ralph and R. A. Buhrman, arXiv:1203.2875.
- [35] M. Morota, Y. Niimi, K. Ohnishi, D. H. Wei, T. Tanaka, H. Kontani, T. Kimura, and Y. Otani, *Phys. Rev. B* **83**, 174405 (2011).
- [36] C. Burrowes, B. Heinrich, B. Kardasz, E.A. Montoya, E. Girt, Y. Sun, Y. Y. Song, and M. Wu, *Appl. Phys. Lett.* **100**, 092403 (2012).
- [37] K. M. Schep, J. B. A. N. van Hoof, P. J. Kelly, G. E. W. Bauer and J. E. Inglesfield, *Phys. Rev. B* **56**, 10805 (1997).
- [38] G.E.W. Bauer, K. M. Schep, K. Xia and P. J. Kelly, *J. Phys. D: Appl. Phys.*, **35**, 2410 (2002).
- [39] K. Ando, S. Takahashi, J. Ieda, Y. Kajiwara, H. Nakayama, T. Yoshino, K. Harii, Y. Fujikawa, M. Matsuo, S. Maekawa, and E. Saitoh, *J. Appl. Phys.*, **109**, 103913 (2011).